Study of the decay $D^0 \to K^- K^- K^+ \pi^+$

E. M. Aitala,[9] S. Amato,[1] J. C. Anjos,[1] J. A. Appel,[5] D. Ashery,[14] S. Banerjee,[5]

I. Bediaga,[1] G. Blaylock,[8] S. B. Bracker,[15] P. R. Burchat,[13] R. A. Burnstein,[6] T. Carter,[5]

H. S. Carvalho,[1] N. K. Copty,[12] L. M. Cremaldi,[9] C. Darling,[18] K. Denisenko,[5] S. Devmal,[3]

A. Fernandez,[11] G. F. Fox,[12] P. Gagnon,[2] S. Gerzon,[14] C. Gobel,[1] K. Gounder,[9]

A. M. Halling,[5] G. Herrera,[4] G. Hurvits,[14] C. James,[5] P. A. Kasper,[6] S. Kwan,[5]

D. C. Langs,[12] J. Leslie,[2] J. Lichtenstadt,[14] B. Lundberg,[5] S. MayTal-Beck,[14] B. Meadows,[3]

J. R. T. de Mello Neto,[1] D. Mihalcea,[7] R. H. Milburn,[16] J. M. de Miranda,[1] A. Napier,[16]

A. Nguyen,[7] A. B. d'Oliveira,[3,11] K. O'Shaughnessy,[2] K. C. Peng,[6] L. P. Perera,[3]

M. V. Purohit,[12] B. Quinn,[9] S. Radeztsky,[17] A. Rafatian,[9] N. W. Reay,[7] J. J. Reidy,[9]

A. C. dos Reis,[1] H. A. Rubin,[6] D. A. Sanders,[9] A. K. S. Santha,[3] A. F. S. Santoro,[1]

A. J. Schwartz,[3] M. Sheaff,[17] R. A. Sidwell,[7] A. J. Slaughter,[18] M. D. Sokoloff,[3] J. Solano,[1]

N. R. Stanton,[7] R. J. Stefanski,[5] K. Stenson,[17] D. J. Summers,[9] S. Takach,[18] K. Thorne,[5]

A. K. Tripathi,[7] S. Watanabe,[17] R. Weiss-Babai,[14] J. Wiener,[10] N. Witchey,[7]

E. Wolin,[18] S. M. Yang,[7] D. Yi,[9] S. Yoshida,[7] R. Zaliznyak,[13] and C. Zhang[7]

(Fermilab E791 Collaboration)

[1] *Centro Brasileiro de Pesquisas Físicas,*

Rio de Janeiro, Brazil

[2] *University of California,*

Santa Cruz, California 95064

[3] *University of Cincinnati,*

Cincinnati, Ohio 45221

[4] *CINVESTAV, Mexico City, Mexico*

[5] *Fermilab, Batavia, Illinois 60510*

[6] *Illinois Institute of Technology,*

Chicago, Illinois 60616

[7] *Kansas State University,*
Manhattan, Kansas 66506
[8] *University of Massachusetts,*
Amherst, Massachusetts 01003
[9] *University of Mississippi-Oxford,*
University, Mississippi 38677
[10] *Princeton University,*
Princeton, New Jersey 08544
[11] *Universidad Autonoma de Puebla,*
Puebla, Mexico
[12] *University of South Carolina,*
Columbia, South Carolina 29208
[13] *Stanford University,*
Stanford, California 94305
[14] *Tel Aviv University, Tel Aviv, Israel*
[15] *Box 1290, Enderby,*
BC, V0E 1V0, Canada
[16] *Tufts University, Medford,*
Massachusetts 02155
[17] *University of Wisconsin,*
Madison, Wisconsin 53706
[18] *Yale University,*
New Haven, Connecticut 06511

(Dated: May 18, 2001)

Abstract

Using data from the E791 fixed-target hadroproduction experiment at Fermilab we have studied the Cabibbo-favored but phase-space suppressed decay, $D^0 \to K^- K^- K^+ \pi^+$. We find the decay rate for this mode to be $(0.54 \pm 0.16 \pm 0.08) \times 10^{-2}$ times that for the normalization mode $D^0 \to K^- \pi^- \pi^+ \pi^+$. We observe a clear signal for $D^0 \to \phi K^- \pi^+$ which is consistent with producing 0.7 ± 0.3 of the $D^0 \to K^- K^- K^+ \pi^+$ signal. In the context of simple models, we use our measurements to estimate the importance of decay amplitudes that produce extra quark-antiquark pairs from the vacuum relative to those that do not.

The decays $D^0 \to K^- K^- K^+ \pi^+$ and $D^0 \to K^- \pi^- \pi^+ \pi^+$ are both Cabibbo-favored, but phase-space suppresses the former relative to the latter. In addition, the decay $D^0 \to K^- K^- K^+ \pi^+$ requires the production of at least one extra quark-antiquark pair, an $s\overline{s}$, either from the vacuum or via a final state interaction. The more common decay $D^0 \to K^- \pi^- \pi^+ \pi^+$ may proceed both via an intermediate state such as $\overline{K}^{*0} \rho^0$ in which the resonant particles contain only quarks produced directly from a spectator amplitude, and via an amplitude that requires the production of at least one extra $q\overline{q}$ pair from the vacuum.

In this paper we present a decay rate measurement for $D^0 \to K^- K^- K^+ \pi^+$ relative to that for $D^0 \to K^- \pi^- \pi^+ \pi^+$ using data from the E791 fixed-target hadroproduction experiment at Fermilab. This allows us to determine the importance of decay amplitudes that produce extra $q\overline{q}$ pairs from the vacuum relative to those that do not. In addition, we study the $K^- K^+$ invariant mass distribution in signal events to search for intermediate ϕ production.

Experimental Overview

Experiment E791 recorded 2×10^{10} interactions during the 1991/92 fixed-target run at Fermilab using a 500 GeV/c π^- beam and an open geometry spectrometer[1] in the Tagged Photon Laboratory. The target consisted of one platinum foil and four diamond foils, separated by gaps of 1.34 to 1.39 cm. Each foil was approximately 0.4% of a pion interaction length thick (0.5 mm for platinum and 1.6 mm for carbon). The average decay length of an 80 GeV D^0 is approximately 5 mm, so most of the D^0's decayed in the air gaps between target foils where backgrounds are lower. Six planes of silicon microstrip detectors (SMDs) and eight proportional wire chambers (PWCs) were used to track the beam particles. The downstream detector consisted of 17 planes of SMDs for vertex detection, 35 drift chamber planes, two PWCs, two magnets for momentum analysis (both bending in the same direction), two multicell threshold Čerenkov counters[2] for charged particle identification (with nominal pion thresholds of 6 GeV/c and 11 GeV/c), electromagnetic and hadronic calorimeters for electron identification and for online triggering, and two planes of muon scintillators. An interaction trigger required a beam particle and an interaction in the target. A very loose transverse energy trigger, based on the energy deposited in the calorimeters, and a fast data acquisition system [3] allowed the experiment to collect data at a rate of 30 Mbytes/s with 50 μs/event dead time and to write data to tape at a rate of 10 Mbytes/s.

Event Selection

Data reconstruction and additional event selection were done using offline parallel processing systems [4]. Events with evidence of well-separated production (primary) and decay (secondary) vertices were retained for further analysis. Candidate $D^0 \to K^- K^- K^+ \pi^+$ and $D^0 \to K^- \pi^- \pi^+ \pi^+$ decays (and their corresponding charge conjugate decays, which we include implicitly whenever we refer to a decay chain) were selected from events with at least one candidate four-prong secondary vertex. Selection criteria (cuts), used for both modes, were determined by optimizing the expected statistical significance of the $D^0 \to K^- K^- K^+ \pi^+$ signal. To avoid bias, we masked the signal region (1.845 GeV/c^2 < mass($K^- K^- K^+ \pi^+$) < 1.885 GeV/c^2) in the real data early in the analysis and systematically studied sensitivity using a combination of real data for background and Monte Carlo simulations for signal. Only after we had determined a set of cuts for the final analysis, and looser and tighter sets of cuts for studies of systematic uncertainties, did we examine the data in the signal region.

We used Monte Carlo simulations of $D^0 \to K^- K^- K^+ \pi^+$ decays and $D^0 \to K^- \pi^- \pi^+ \pi^+$ real data to estimate the efficiencies of potential cuts. We compared Monte Carlo simulations of $D^0 \to K^- \pi^- \pi^+ \pi^+$ to the real data in this channel to validate our Monte Carlo. Where the distributions in the Monte Carlo simulation of $D^0 \to K^- \pi^- \pi^+ \pi^+$ match the real data, we trust the $D^0 \to K^- K^- K^+ \pi^+$ Monte Carlo simulation. Where the distributions in the Monte Carlo simulation of $D^0 \to K^- K^- K^+ \pi^+$ match those in the Monte Carlo simulation of $D^0 \to K^- \pi^- \pi^+ \pi^+$, we trust that the corresponding distributions observed for real $D^0 \to K^- \pi^- \pi^+ \pi^+$ correctly predict those for $D^0 \to K^- K^- K^+ \pi^+$. At this stage, we estimated the background within the signal region by interpolating linearly from sidebands in the $K^- K^- K^+ \pi^+$ invariant mass distribution of the data.

When events were initially reconstructed, a topological vertexing algorithm was used to identify a primary (interaction) vertex and possible secondary (downstream) vertices. Our D^0 candidates are constructed from four-track secondary vertices (referred to as 'SEED4' candidates) and from three-track secondary vertices with the addition of a fourth track (referred to as 'SEED3' candidates). Because the initial topological vertexing algorithm assigned each track to one vertex candidate, and because it was optimized for two-body and three-body charm decays, about half of our signal comes from the SEED4 sample and half from the SEED3 sample.
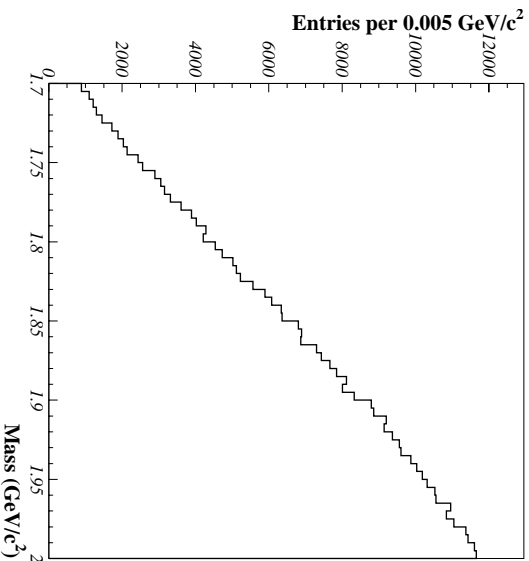
5

FIG. 1: $KK\bar{K}\pi$ invariant mass distributions after the preliminary event selection

The signal was expected to be small (between 10 and 50 signal events, depending on cuts and allowing for some uncertainty in the relative branching ratio), and the signal-to-background ratio is better in the SEED4 sample when all other cuts are fixed, so the cuts are studied separately for SEED4 and SEED3 candidates. Within each category, we made initial, very loose cuts on a series of candidate variables, primarily informed by our prior experience with similar analyses. The invariant mass distribution of all candidates surviving these loose cuts is shown in Fig. 1. At this point in the analysis we decided to proceed blindly: to mask the signal region in the data and optimize sensitivity as discussed in detail below.

As part of the optimization, we create combined figure-of-merit (FOM) variables from kinematic and particle identification variables that are essentially independent of each other in our Monte Carlo simulations and in the $D^0 \rightarrow K^-\pi^-\pi^+\pi^+$ data. For each of the SEED4 and SEED3 samples, we start with a set of independent cuts on individual variables, and then construct combined FOM variables for each of the surviving events. The procedure for constructing FOM variables will be described in detail after a discussion of the most important variables used in selecting candidates.

The decay vertex is required to lie outside the target foils and other solid material and to be well-separated from the primary vertex, with $\Delta z > 10\sigma_z$ for SEED4 candidates (where

σ_z is the error on Δz, the longitudinal separation between two vertices) and with $\Delta z > 12\,\sigma_z$ for SEED3 candidates. The transverse momentum of the D^0 candidate with respect to the line-of-flight defined by the secondary and primary vertex positions (p_T-balance) is required to be less than 250 MeV/c. The transverse distance of closest approach of the D^0's line-of-flight with respect to the primary vertex point (denoted DIP) is required to be less than 60 μm. Because vertex separation, transverse momentum imbalance, and DIP correlate strongly, we use a very loose DIP cut at this stage of the analysis and include only DIP, of these variables, in FOM.

The sum of the squares of the momenta of the individual tracks with respect to the D^0 momentum vector discriminates between signal and background when normalized to the maximum value possible for a candidate's reconstructed mass. (This normalization is required to avoid kinematic biases that could artificially create a signal by preferentially increasing the acceptance in the signal region relative to acceptance nearby in mass.) This ratio is required to be greater than 0.2 for the SEED4 candidates and greater than 0.3 for the SEED3 candidates. The product of the ratios of the four daughter tracks' transverse separations from the secondary vertex relative to their transverse separations from the primary vertex is required to be less than 0.005 for SEED4 and SEED3 candidates. The maximum ratio for a single track is required to be less than 1.0 and is included in FOM for SEED3 candidates; this is unnecessary for SEED4 candidates because their distribution was cleaner upon initial selection.

To avoid problems due to congestion near the primary vertex, we also found it useful to require either an absolute separation of the primary and secondary vertex candidates or that the secondary vertex be "isolated" from other tracks by requiring that all other tracks pass at least a minimum distance from the secondary vertex candidate. The Monte Carlo simulation fails to describe the distribution of additional tracks in the events sufficiently well, so we base these cuts, and the associated efficiencies, on studies of the real $D^0 \to K^-\pi^-\pi^+\pi^+$ data. For SEED4 candidates we require either vertex separation greater than 0.5 cm or secondary vertex isolation greater than 20 μm. For SEED3 candidates we require either vertex separation greater than 0.5 cm or secondary vertex isolation greater than 80 μm.

Our particle identification algorithm compared the light observed in the two multicell threshold Čerenkov detectors with that expected for the five hypotheses e, μ, π, K, and p for each track. It then assigned a probability to each hypothesis, including *a priori*

likelihoods for each species, so that the sum of probabilities for each track added to unity. Tracks that are π/K ambiguous had K probabilities near 0.13. Similarly, those that are K/p ambiguous had K probabilities near 0.80. Each kaon candidate is required to have K probability greater than 0.20. The three K probabilities are also included in FOM as independent variables. Our Monte Carlo simulation of the Čerenkov identification does not match our data's variation with transverse momentum well; furthermore, the Monte Carlo distributions of K probability for the kaons in $D^0 \to K^- K^- K^+ \pi^+$ and $D^0 \to K^- \pi^- \pi^+ \pi^+$ decays differ. In calculating the Čerenkov probabilities' contributions to FOM, for each range of K probability we use the average of the fraction found in the $D^0 \to K^- K^- K^+ \pi^+$ Monte Carlo simulation and in the real data's $D^0 \to K^- \pi^- \pi^+ \pi^+$ signal. We also considered using the product of the three K probabilities in FOM, but found that the greatest sensitivity could be achieved using them independently. Because most tracks are pions, we found no benefit in using Čerenkov identification for the pions.

Two more variables provide some discriminating power between signal and background. In the Monte Carlo simulation, there were no SEED4 signal events with proper decay time greater than 3.5 ps; in the data, background was observed in this region. So we removed SEED4 events with proper decay time greater than 3.5 ps. SEED3 signal events extended past 3.5 ps, but we could not find a cut that improved the sensitivity. For both SEED4 and SEED3 events, we found that the distribution of the cosine of the polar angle of the sphericity axis of the candidate relative to the candidate's line-of-flight discriminated between signal and background, primarily because background accumulates preferentially at values of the cosine near one. This correlates with the scaled, summed transverse momentum squared being small. Having made an absolute cut on the latter quantity, the cosine of the sphericity angle is included in FOM for both the SEED4 and SEED3 samples.

To create FOM variables, we divided the distribution for any one variable into four or five ranges and determined the fraction of signal that appeared in each range. Similarly, we determined from the data what fraction of background appeared in each range. We use $\mathcal{S}_{A,i}$ to denote the probability that a signal event falls in range i for variable A. We use $\mathcal{B}_{A,i}$ for background similarly. For example, if three variables A, B, and C are used to define FOM, and they are observed in ranges i, j, and k respectively, we calculate:

$$\mathrm{FOM} = \frac{\mathcal{S}_{A,i}\mathcal{S}_{B,j}\mathcal{S}_{C,k}}{\mathcal{B}_{A,i}\mathcal{B}_{B,j}\mathcal{B}_{C,k}} \ . \tag{1}$$

This is effectively a ratio of likelihoods constructed as a product of independent relative probabilities. Assuming the variables A, B, and C are statistically independent, an event's FOM is the relative signal-to-background ratio in the i, j, k cell of A, B, C phase-space: the signal-to-background ratio in that cell will be the signal-to-background ratio before FOM cuts times FOM. In selecting events using FOM, we accept events with FOM greater than a given value and reject those with lower values.

The FOM distributions for SEED4 and SEED3 Monte Carlo signal and for real data in the sidebands (after all the non-FOM cuts) are shown in Fig. 2. The background accumulates preferentially at lower values of FOM, while the signal populates the FOM distribution much more uniformly. In determining where to cut on FOM, we calculate the expected $KKK\pi$ signal using (i) our observed $K^-\pi^-\pi^+\pi^+$ signal, (ii) the ratio of decay rates previously reported by E687[6], and (iii) the relative reconstruction efficiencies determined from our Monte Carlo simulations. We calculate the background expected in a 15 MeV/c^2 window by extrapolating the $K^-K^-K^+\pi^+$ rate from outside our masked-off range (1845 - 1885 MeV/c^2). With no FOM cuts, these assumptions predict 6.1 SEED4 and 7.5 SEED3 signal events with 4.0 and 7.2 background events, respectively. Adding these together predicts $S/B = 1.2$, $S/\sqrt{B} = 4.1$, and $S/\sqrt{S+B} = 2.7$. Our final selection of cuts balances our interests in maximizing the $S/\sqrt{S+B}$, maximizing $S/\sqrt{B}$, and maintaining good S/B ratios in the SEED4 and SEED3 samples. Our final selection of cuts is FOM > 0.5 for SEED4 candidates and FOM > 1.0 for SEED3 candidates. With these cuts our algorithm predicts 11.5 signal events and 3.1 background, giving $S/B = 3.7$, $S/\sqrt{B} = 6.5$, and $S/\sqrt{S+B} = 3.0$.

Several points deserve emphasis. The technique for selecting cuts is almost unbiased. The data in the $D^0 \to K^-K^-K^+\pi^+$ signal region have not been examined, so we avoid choices which are subconsciously chosen to either enhance the signal level or increase the sensitivity of an upper limit should no signal be observed. The potential bias in selecting cuts while looking at the background outside the signal region is small; this will be quantified when we discuss systematic errors. Using FOM to combine variables that discriminate between signal and background allows us to create a relatively robust variable, $S/\sqrt{S+B}$, which correlates with our ability to measure the decay rate and varies slowly with changes in FOM cuts. We can choose looser and tighter cuts for which S/B will vary substantially, but $S/\sqrt{S+B}$ should not. This allows us to examine the data *a posteriori* to identify potential problems
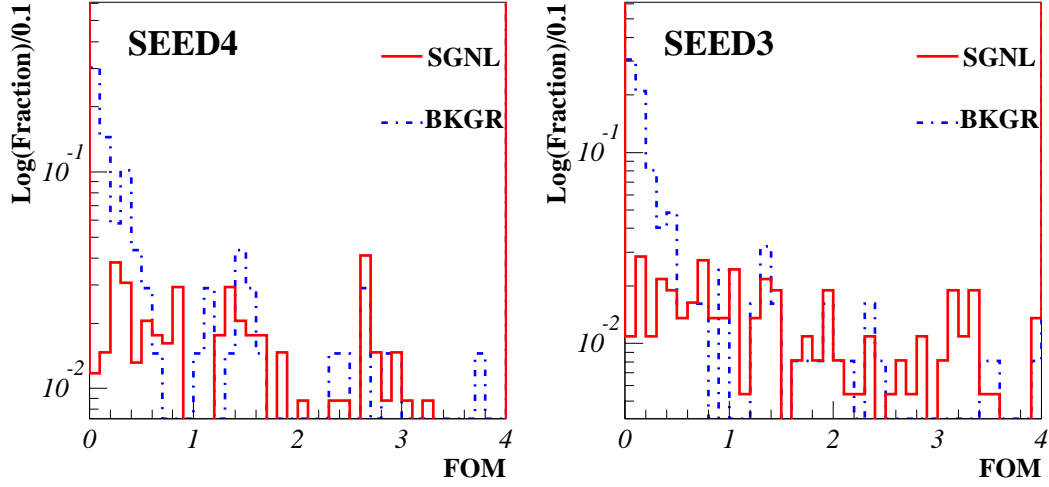
FIG. 2: Figure-of-merit (FOM) distributions for Monte Carlo signal (solid lines) and for background (dashed lines) for SEED4 candidates (on the left) and SEED3 candidates (on the right), after all cuts on individual variables, as discussed in the text.

with the analysis.

Branching Ratio Measurement

The $K^-K^-K^+\pi^+$ invariant mass distribution for events satisfying the final set of cuts described above is shown in Fig. 3, and the $K^-\pi^-\pi^+\pi^+$ invariant mass distribution used for normalization is shown in Fig. 4. The cuts used for the normalization sample correspond closely to those used for the $K^-K^-K^+\pi^+$ sample without FOM cuts. The detailed requirements for finding the vertex outside the target foils or other solid material, and an additional requirement that the $K^-\pi^-\pi^+\pi^+$ daughter tracks not point back to the primary vertex, differ slightly because the Q-values of the two decays (summed kinetic energies of the decay products) differ substantially. Parameters for the $K^-K^-K^+\pi^+$ invariant mass distribution are determined using an unbinned maximum likelihood fit in which the signal is described as a Gaussian with the mass and width allowed to float and the background is described as a quadratic function. Parameters for the $K^-K^-K^+\pi^+$ Monte Carlo data as well as for the $K^-\pi^-\pi^+\pi^+$ real and Monte Carlo data are determined using binned maximum likelihood fits in which the signals are described as Gaussian distributions with masses and widths
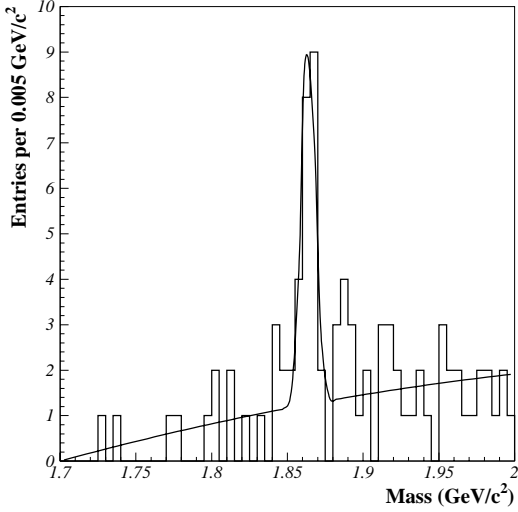
FIG. 3: The $KKK\pi$ invariant mass distribution for events satisfying the final selection criteria. The SEED4 and SEED3 samples have been combined. The fitted signal level is 18.4 ± 5.3 events.
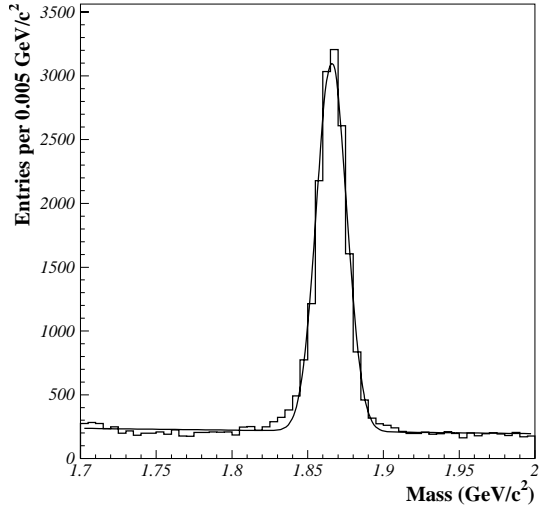

FIG. 4: The $K\pi\pi\pi$ invariant mass distribution for events satisfying the selection criteria described in the text. These criteria are similar to those used for the $KKK\pi$ candidates to reduce the systematic uncertainties in determining the relative branching ratio. The fitted signal level is 14472 ± 134 events.

allowed to float and the backgrounds are described as linear functions. The quadratic term found in fitting the $K^-K^-K^+\pi^+$ is small, but we allow this extra degree of freedom to be conservative. The Monte Carlo data has essentially no background, and adding a quadratic term to the $K^-\pi^-\pi^+\pi^+$ fit makes a negligibly small difference, so for the Monte Carlo and normalization samples we present the results of fits with only linear background terms. The results of these fits are summarized in Table I. The $K^-K^-K^+\pi^+$ signal level is 18.4 ± 5.3 events.

To convert this signal level into a ratio of decay rates we need the $K^-\pi^-\pi^+\pi^+$ signal level (14472 ± 134 events) and the relative efficiency for the two decay modes. The latter differs from unity for three reasons. First, the Q-value for the $KKK\pi$ decay is smaller than that for the $K\pi\pi\pi$ decay. This leads to very different track opening angles, and hence to very different vertex resolutions. As a result, vertex reconstruction efficiencies and vertex

11

		Signal	Mass	Width
real data	$KKK\pi$	18.4 ± 5.3	1.8639 ± 0.0015	0.0045 ± 0.0014
	$K\pi\pi\pi$	14472 ± 134	1.8658 ± 0.0001	0.0100 ± 0.0001
Monte Carlo	$KKK\pi$	595 ± 26	1.8646 ± 0.0002	0.0041 ± 0.0001
	$K\pi\pi\pi$	2156 ± 48	1.8644 ± 0.0002	0.0082 ± 0.0002

TABLE I: Parameters determined by fitting the final real data and Monte Carlo $KKK\pi$ and $K\pi\pi\pi$ samples as described in the text. Each Monte Carlo sample was generated with 500,000 events. The errors quoted are statistical only.

separation distributions differ. Second, the background in the $KKK\pi$ sample is reduced using FOM cuts, a procedure not necessary in the normalization sample. Finally, the $KKK\pi$ sample has two additional kaons, which reduces the particle identification efficiency. We start with the relative efficiency determined from the Monte Carlo simulations, 0.275 ± 0.013, (where the reported error is the statistical uncertainty from the Monte Carlo samples) and make corrections to account for differences between real data and Monte Carlo data observed using the $D^0 \to K^-\pi^-\pi^+\pi^+$ signal. These corrections are summarized in Table II. Taken together, we estimate the efficiency for $D^0 \to K^-K^-K^+\pi^+$ relative to that for $D^0 \to K^-\pi^-\pi^+\pi^+$ to be 15% less than that determined directly from the Monte Carlo simulations.

The significant sources of systematic uncertainty in the ratio of decay rates are summarized in Table III. Each of the correction factors described above has a corresponding uncertainty determined by studying the $D^0 \to K^-\pi^-\pi^+\pi^+$ data that pass cuts, and the Monte Carlo samples for both decay modes. The Monte Carlo statistics contribute a 4.7% uncertainty. Systematic differences in tracking and vertexing efficiencies between real data and Monte Carlo samples have been studied previously[5]. They contribute an additional 5% systematic uncertainty beyond that determined for the correction factors; this is effectively an uncertainty on the relative efficiency for the loosest cuts used. We vary the fit used to extract the number of $D^0 \to K^-K^-K^+\pi^+$ signal events allowing both linear and quadratic backgrounds, fixed and floating masses, and fixed and floating Gaussian width, and all possible combinations. The number of signal events ranges from 17.6 ± 4.7 to 18.8 ± 5.2. Each fit describes the data adequately – for each fit the χ^2 per degree of freedom is less than one. We investigated backgrounds due to misidentified charm decays using Monte Carlo

systematic variation due to	raise $\epsilon_{KKK\pi_{rel}}$ by	correction factor
kaon Čerenkov efficiency	-18%	0.82
SEED4 and SEED3 fractions	$+2.5\%$	1.025
vertex separation	$+1.1\%$	1.011
p_T-balance	$+0.5\%$	1.005
total correction factor	-15%	0.85

TABLE II: Summary of corrections to the relative efficiency from Monte Carlo for reconstructing $KKK\pi$ and $K\pi\pi\pi$ final states. The relative efficiency used for determining the relative branching ratio, $\Gamma_{KKK\pi}/\Gamma_{K\pi\pi\pi}$, will be 0.85 times that found from the Monte Carlo. The total correction factor has been calculated by multiplying the individual correction factors.

simulations and found the overall shape to agree well with that found in the fits. We could associate a systematic uncertainty of 4.3% with our fitting procedure; this would cover the largest excursion of the fit results from the central value reported. Because the background near the signal region may be higher than predicted by our fit over the whole range shown, we considered several piece-wise linear fits as well. We estimate an additional one event systematic uncertainty in the background level which we add in quadrature to give a total systematic uncertainty of 7.6% due to the shapes of the signal and background.

With the corrected relative efficiency described above, and adding the systematic uncertainties in quadrature, the ratio of decay rates is:

$$\frac{\Gamma(D^0 \rightarrow K^- K^- K^+ \pi^+)}{\Gamma(D^0 \rightarrow K^- \pi^- \pi^+ \pi^+)} = (0.54 \pm 0.16 \pm 0.08) \times 10^{-2} \ . \tag{2}$$

The first error is statistical; the second is systematic. Using the $D^0 \rightarrow K^- \pi^- \pi^+ \pi^+$ branching ratio reported by the Particle Data Group[7], $(7.6 \pm 0.4)\%$, and folding its error into our final systematic uncertainty, we obtain

$$\mathcal{BR}(D^0 \rightarrow K^- K^- K^+ \pi^+) = (4.1 \pm 1.2 \pm 0.6) \times 10^{-4} \ . \tag{3}$$

The ratio of decay rates reported by E687 is $(0.28\pm0.07\pm0.01)\%$[6]. The difference between our result and the E687 result is $(0.26 \pm 0.19)\%$. The fractional errors for the two results are 0.32 (this work) and 0.25 (E687) where the statistical and systematic errors have been added in quadrature.

differences between Monte Carlo and real data (after corrections):	
kaon Čerenkov efficiency	10%
tracking and vertexing efficiencies	5%
SEED4 and SEED3 fractions	1.8%
vertex seapartion requirement	1.1%
p_T-balance	0.5%
sub total	11.4%
Statistical fluctuations in Monte Carlo data, including difference between non-resonant and $\phi K\pi$	4.7%
Signal and background shapes	7.6%
FOM predictions	1.5%
Total (added in quadrature)	14.6%

TABLE III: Summary of systematic errors. The total has been calculated by adding the individual contributions in quadrature.

Search for Resonant Substructure

Two or more of the final state hadrons in a $D^0 \to K^-K^-K^+\pi^+$ final state might be the decay products of an intermediate resonance. The signal observed in this experiment is small, and the phase-space so small that it will distort the shapes of broad resonances that appear as intermediate states. Hence, we have not attempted a coherent amplitude analysis similar to the analysis we did for the decay $D^0 \to K^-K^+\pi^-\pi^+$[8] or similar to the incoherent amplitude analysis done by MARK III for the decay $D^0 \to K^-\pi^-\pi^+\pi^+$[9]. Rather, we have looked only at K^-K^+ invariant mass distributions of $D^0 \to K^-K^-K^+\pi^+$ candidates (two pairs per candidate). The signal distribution (for events with 1.855 GeV/c^2 $< m(K^-K^-K^+\pi^+) < 1.875$ GeV/c^2), seen in Fig. 8, shows an accumulation of entries near the ϕ mass. In comparison, the corresponding distribution for background events in the ranges 1.700 GeV/c^2 $< m(KKK\pi) < 1.845$ GeV/c^2 and 1.885 GeV/c^2 $< m(KKK\pi) <$ 2.000 GeV/c^2, seen in Fig. 9, has a much broader distribution, with only a hint of any structure at low mass.

To understand the nature of our signal better, we generated two Monte Carlo samples. In our non-resonant $D^0 \to K^-K^-K^+\pi^+$ simulation, the generated events populate four-body phase-space uniformly. In our $D^0 \to \phi K^-\pi^+$; $\phi \to K^-K^+$ simulation, the generated events populate the (ϕ, K, π) three-body phase-space uniformly. Both Monte Carlo samples are

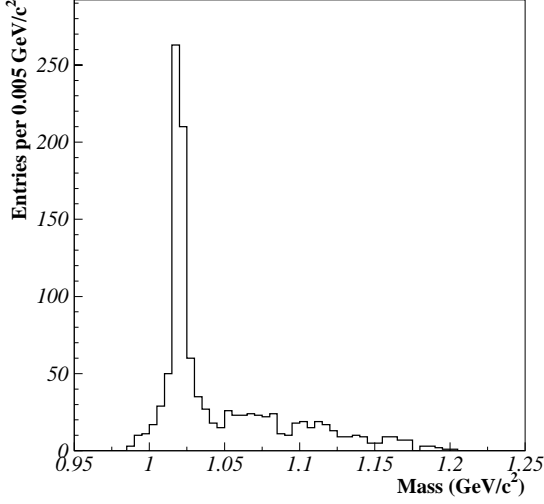FIG. 5: K^-K^+ invariant mass distribution for $D^0 \to \phi K \pi$ Monte Carlo events. There are two entries per D^0 candidate.
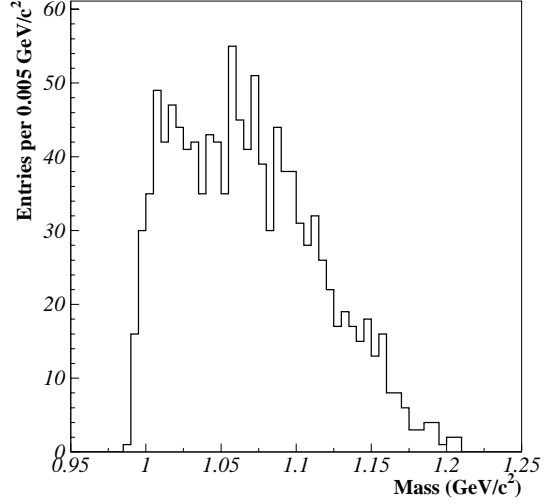

FIG. 6: K^-K^+ invariant mass distribution for non-resonant $D^0 \to K^-K^-K^+\pi^+$ Monte Carlo events. There are two entries per D^0 candidate.

fully simulated and then reconstructed and analyzed as were the real data. The K^-K^+ invariant mass distributions corresponding to those for the real data are shown in Figs. 5 and 6. The two distributions differ qualitatively.

Without trying to do a real amplitude analysis, we fit the K^-K^+ invariant mass distribution of Fig. 8 as an incoherent sum of the shapes of the two Monte Carlo models and of the background region. We use a binned maximum likelihood fit in which the two signal fractions float freely and the background fraction floats, but we add a term to the likelihood function to account for the difference between the background fraction and that determined from the earlier fit of the $KKK\pi$ used for the branching ratio measurement. This fit (which is superposed on the data in Fig. 8) finds that 0.7 ± 0.3 of the $KKK\pi$ signal comes from $\phi K \pi$ decay. This result indicates that intermediate ϕ production is an important mechanism in $D^0 \to K^-K^-K^+\pi^+$ decay.

Interpretation of the Relative Branching Ratio

The relative branching ratio determined in Eq. 2 is small primarily because the Q-value of the $KKK\pi$ decay is much less than that of the $K\pi\pi\pi$ decay. The phase space for non-resonant four-body $KKK\pi$ decay, $\Omega_{KKK\pi}$, is only 1.43×10^{-2} times that for non-resonant

four-body $K\pi\pi\pi$ decay, $\Omega_{K\pi\pi\pi}$. If one assumes that both decays are purely non-resonant, the ratio of invariant matrix elements, $\mathcal{R}$, is a constant and can be determined using

$$\frac{\Gamma_{KKK\pi}}{\Gamma_{K\pi\pi\pi}} = \frac{\Omega_{KKK\pi}}{\Omega_{K\pi\pi\pi}} \times \mathcal{R} \tag{4}$$

to be $\mathcal{R} = 0.32 \pm 0.10$.

Neither decay is purely non-resonant, but we can use the value of $\mathcal{R}$, determined using this equation, to estimate crudely the importance of amplitudes in which at least one $q\bar{q}$ pair is produced from the vacuum. The decay $D^0 \to K^- \pi^- \pi^+ \pi^+$ can proceed via amplitudes in which the quarks produced in a spectator decay coalesce to form hadrons which, in turn, decay strongly to produce four hadrons in the final state. The decay $D^0 \to K^- K^- K^+ \pi^+$ cannot proceed via such amplitudes. It requires either that an extra $s\bar{s}$ pair be produced from the vacuum or that long distance final state interactions of hadrons produced at short distances produce such pairs. Feynman diagrams for such amplitudes are shown in Fig. 7, along with those of corresponding amplitudes for $D^0 \to K^- \pi^- \pi^+ \pi^+$ decays where an extra $u\bar{u}$ or $d\bar{d}$ pair is produced.

Accounting for the differences in phase spaces using $\Omega_{KKK\pi}/\Omega_{K\pi\pi\pi}$, and ignoring any possible quantum mechanical intereferences, one can write $\mathcal{R}$ in terms of the probabilities that the final states we are considering are produced by amplitudes in which a $q\bar{q}$ state is produced from the vacuum, $P_{u\bar{u}}$, $P_{d\bar{d}}$, $P_{s\bar{s}}$ for $u\bar{u}$, $d\bar{d}$, and $s\bar{s}$ respectively, or in which the amplitude has no pair produced from the vacuum, $P_{\text{no pair}}$. As a first approximation, one can imagine a form of isospin symmetry in which $P_{d\bar{d}} = P_{s\bar{s}}$ for each amplitude that can lead to four charged hadrons in the final state and the corresponding $u\bar{u}$ amplitude does not lead to four charged hadrons in the final state. In this case we calculate

$$\mathcal{R} = 0.32 = \frac{P_{s\bar{s}}}{P_{s\bar{s}} + P_{\text{no pair}}} \tag{5}$$

in which case

$$\frac{P_{s\bar{s}}}{P_{\text{no pair}}} = 0.47 \ . \tag{6}$$

If the amplitudes for producing each flavor of $q\bar{q}$ pair are the same, and the likelihoods for producing four charged hadrons in the final state are the same (allowing for resonant three-body decays as well as for non-resonant four-body decay), then one might expect $P_{u\bar{u}} = P_{d\bar{d}} = P_{s\bar{s}}$. In this case

$$\frac{P_{s\bar{s}}}{P_{\text{no pair}}} = 0.90 \ . \tag{7}$$

16

If the amplitudes with $u\overline{u}$ and $d\overline{d}$ pairs produced from the vacuum somehow interfere destructively so that the $D^0 \rightarrow K^- \pi^- \pi^+ \pi^+$ decay rate is equal to that which would be produced in the absence of these additional amplitudes, $\mathcal{R}$ is a direct measurement of

$$\frac{P_{s\overline{s}}}{P_{\text{no pair}}} = 0.32 \ . \tag{8}$$

A simple measurement of $\Gamma(D^0 \rightarrow K^- K^- K^+ \pi^+)/\Gamma(D^0 \rightarrow K^- \pi^- \pi^+ \pi^+)$ cannot tell us which picture is closest to the truth, although it seems likely that $0.3 < P_{s\overline{s}}/P_{\text{no pair}} < 0.9$.

Summary

Using data from Fermilab experiment E791, we have studied the decay $D^0 \rightarrow K^- K^- K^+ \pi^+$. To avoid bias, the selection criteria for the $K^- K^- K^+ \pi^+$ candidates were determined "blindly" – we masked the signal region in the real data and systematically studied sensitivity using a combination of real data for background, and Monte Carlo simulations and real data in the normalization decay mode $D^0 \rightarrow K^- \pi^- \pi^+ \pi^+$ for signal. Only after we had determined the final set of cuts did we examine the data in the signal region. We observe a signal of 18.4 ± 5.3 events from which we find the ratio of decay rates $\Gamma(D^0 \rightarrow K^- K^- K^+ \pi^+)/\Gamma(D^0 \rightarrow K^- \pi^- \pi^+ \pi^+)$ to be $(0.54 \pm 0.16 \pm 0.08)\%$. We also have examined the $K^- K^+$ invariant mass distribution of signal events looking for evidence of resonant substructure, i.e., $D^0 \rightarrow \phi K^- \pi^+$; $\phi \rightarrow K^- K^+$. Fitting the distribution using an incoherent sum of resonant and non-resonant signal shapes plus a background shape, we find that 0.7 ± 0.3 of the signal comes from $\phi K \pi$. Finally, using the ratio of non-resonant phase-spaces for the two decays as an approximation for the correctly weighted ratio, we find the ratio of matrix elements that lead to the signal and normalization final states to be $\mathcal{R} = 0.32 \pm 0.10$. Producing $D^0 \rightarrow K^- K^- K^+ \pi^+$ requires producing an extra $s\overline{s}$ pair from the vacuum or in a final state interaction. Relating this probability to $\mathcal{R}$ is highly model-dependent, and our measurement does not suffice to distinguish among models. However, it seems likely that $0.3 < P_{s\overline{s}}/P_{\text{no pair}} < 0.9$.

Acknowledgements

REFERENCES

[1] E791 Collaboration, E. M. Aitala *et al.*, Eur. Phys. J.direct **C4**, 1 (1997); J. A. Appel, Ann. Rev. Nucl. Part. Sci. **42**, 367 (1992), and references therein; D. J. Summers *et al.*, in: Proceedings of the *XXVII* th *Rencontre de Moriond*, Electroweak Interactions and Unified Theories, Les Arc, France, 417 (1992).

[2] D. Bartlett *et al.*, Nucl. Instr. and Meth. **A260**, 55 (1986).

[3] S. Amato *et al.*, Nucl. Instr. and Meth. **A324**, 535 (1993).

[4] F. Rinaldo and S. Wolbers, Computers in Physics **7**, 184 (1993); S. Bracker *et al.*, IEEE Trans. Nucl. Sci. **43**, 2457 (1996).

[5] E791 Collaboration, E. M. Aitala *et al.*, Phys. Lett **B462**, 401 (1999).

[6] E687 Collaboration, L. Frabetti *et al.*, Phys. Lett. **B354**, 486 (1995).

[7] Review of Particle Physics, R. M. Barnett *et al.*, Phys. Rev. D **54**, 455 (1996).

[8] E791 Collaboration, E. Aitala *et al.*, Phys. Lett. **B423**, 185 (1998).

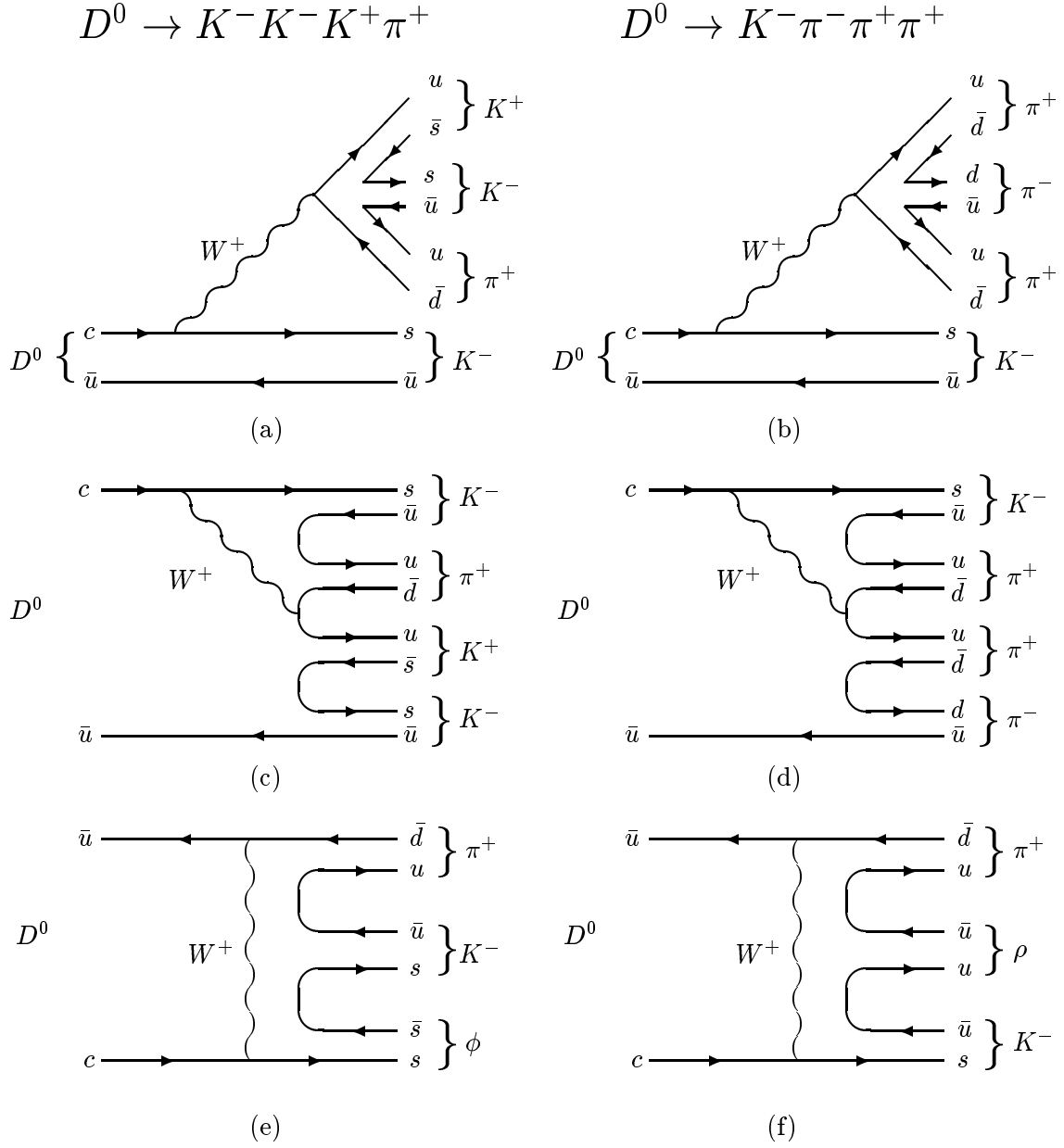[9] MARK III Collaboration, D. Coffman *et al.*, Phys. Rev. D **45**, 2196 (1992).

FIG. 7: Feynman diagrams for amplitudes that can contribute to the decays $D^0 \to K^- K^- K^+ \pi^+$ and $D^0 \to K^- \pi^- \pi^+ \pi^+$. When one light quark pair (either $d\bar{d}$ or $u\bar{u}$) in the latter is replaced by an $s\bar{s}$ pair, we get the former.
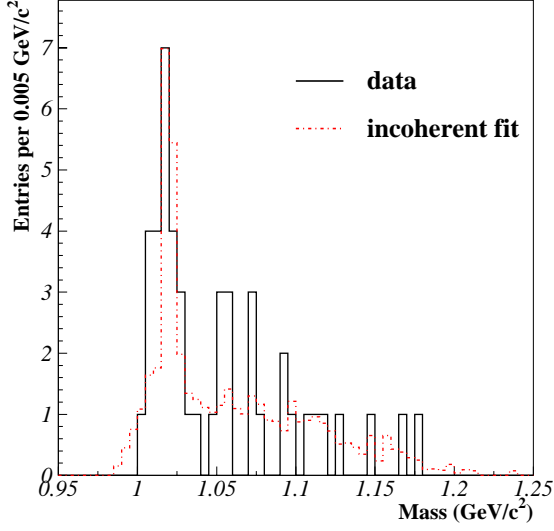
FIG. 8: $K^- K^+$ invariant mass distributions for candidates with 1.855 GeV/c^2 < $m(K^- K^- K^+ \pi^+)$ < 1.875 GeV/c^2. There are two entries per D^0 candidate. The solid line histogram is the real data. The dashed line histogram is a toy model in which the signal fraction is described as 70% from $\phi K \pi$ and 30% non-resonant, and the background scaled from the data, as discussed in the text.
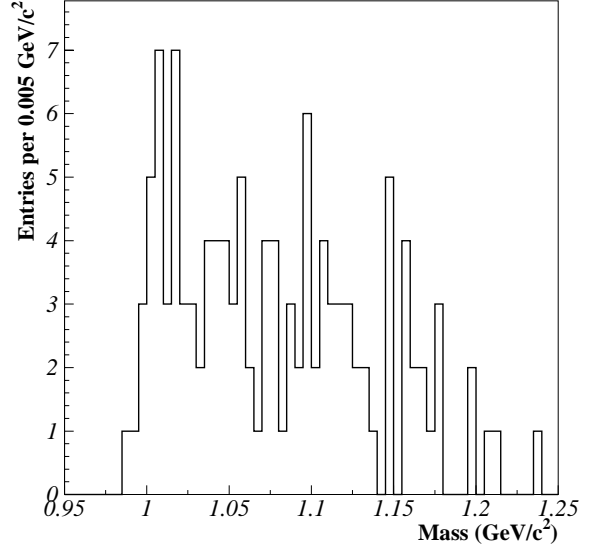

FIG. 9: $K^- K^+$ invariant mass distribution for candidates in the background region. There are two entries per $K^- K^- K^+ \pi^+$ candidate.